



HAL
open science

Increased population exposure to Amphan-scale cyclones under future climates

Dann Mitchell, Laurence Hawker, James Savage, Rory Bingham, Natalie S Lord, Md Jamal Uddin Khan, Paul Bates, Fabien Durand, Ahmadul Hassan, Saleemul Huq, et al.

► **To cite this version:**

Dann Mitchell, Laurence Hawker, James Savage, Rory Bingham, Natalie S Lord, et al.. Increased population exposure to Amphan-scale cyclones under future climates. *Climate Resilience and Sustainability*, 2022, 1 (2), pp.104695. 10.1002/cli2.36 . ird-04554382

HAL Id: ird-04554382

<https://ird.hal.science/ird-04554382>


Submitted on 22 Apr 2024

HAL is a multi-disciplinary open access archive for the deposit and dissemination of scientific research documents, whether they are published or not. The documents may come from teaching and research institutions in France or abroad, or from public or private research centers.

L'archive ouverte pluridisciplinaire **HAL**, est destinée au dépôt et à la diffusion de documents scientifiques de niveau recherche, publiés ou non, émanant des établissements d'enseignement et de recherche français ou étrangers, des laboratoires publics ou privés.

ORIGINAL ARTICLE

Increased population exposure to Amphan-scale cyclones under future climates

Dann Mitchell^{1,2}  | Laurence Hawker^{1,2} | James Savage³ | Rory Bingham^{1,2} | Natalie S. Lord^{1,2} | Md Jamal Uddin Khan⁴ | Paul Bates^{1,2,3} | Fabien Durand^{4,5} | Ahmadul Hassan⁶ | Saleemul Huq⁷ | Akm Saiful Islam⁸ | Yann Krien⁹ | Jeffrey Neal^{1,2,3} | Chris Sampson³ | Andy Smith³ | Laurent Testut⁹ 

¹Cabot Institute for the Environment, University of Bristol, Bristol, UK

²School of Geographical Sciences, University of Bristol, Bristol, UK

³Fathom, Bristol, UK

⁴LEGOS UMR5566, CNRS/CNES/IRD/UPS, Toulouse, France

⁵Laboratório de Geoquímica, Instituto de Geociências, Universidade de Brasília, Brasília, Brazil

⁶Red Cross Red Crescent Climate Centre (RCCC), Dhaka, Bangladesh

⁷International Centre for Climate Change and Development (ICCCAD), Independent University, Bangladesh (IUB), Dhaka, Bangladesh

⁸Institute of Water and Flood Management (IWFM), Bangladesh University of Engineering and Technology (BUET), Dhaka, Bangladesh

⁹LIENSs UMR 7266 CNRS, University of La Rochelle, La Rochelle, France

Correspondence

Dann Mitchell, Cabot Institute for the Environment, University of Bristol, Bristol, BS8 1SS, UK.
 Email: d.mitchell@bristol.ac.uk

Funding information

NERC fellowship, Grant/Award Number: NE/N014057/1; EMERGENCE, Grant/Award Number: NE/S005242/1; Agence Nationale de la Recherche; ANR, Grant/Award Number: ANR-17-CE03-0001; GENCI. JN and LH are, Grant/Award Numbers: NE/S003061/1, NE/S006079/1

Abstract

Southern Asia experiences some of the most damaging climate events in the world, with loss of life from some cyclones in the hundreds of thousands. Despite this, research on climate extremes in the region is substantially lacking compared to other parts of the world. To understand the narrative of how an extreme event in the region may change in the future, we consider Super Cyclone Amphan, which made landfall in May 2020, bringing storm surges of 2–4 m to coastlines of India and Bangladesh. Using the latest CMIP6 climate model projections, coupled with storm surge, hydrological, and socio-economic models, we consider how the population exposure to a storm surge of Amphan's scale changes in the future. We vary future sea level rise and population changes consistent with projections out to 2100, but keep other factors constant. Both India and Bangladesh will be negatively impacted, with India showing >200% increased exposure to extreme storm surge flooding (>3 m) under a high emissions scenario and Bangladesh showing an increase in exposure of >80% for low-level flooding (>0.1 m). It is only when we follow a low-emission scenario, consistent with the 2°C Paris Agreement Goal, that we see no real change in Bangladesh's

This is an open access article under the terms of the [Creative Commons Attribution](https://creativecommons.org/licenses/by/4.0/) License, which permits use, distribution and reproduction in any medium, provided the original work is properly cited.

© 2022 The Authors. *Climate Resilience and Sustainability* published by John Wiley & Sons Ltd on behalf of Royal Meteorological Society.

storm surge exposure, mainly due to the population and climate signals cancelling each other out. For India, even with this low-emission scenario, increases in flood exposure are still substantial (>50%). While here we attribute only the storm surge flooding component of the event to climate change, we highlight that tropical cyclones are multifaceted, and damages are often an integration of physical and social components. We recommend that future climate risk assessments explicitly account for potential compounding factors.

KEYWORDS

attribution, climate change, extreme weather, projections, tropical cyclone, vulnerability

1 | INTRODUCTION

Tropical cyclones pose the largest environmental risk to the countries bordering the Bay of Bengal, with Bangladesh in particular seeing cyclone-related deaths an order of magnitude higher than any other country in the world (Shultz et al., 2005). One of the world's most lethal recorded natural disasters, Cyclone Bhola which hit Bangladesh in 1970, led to over half a million lives lost. There have been numerous other examples of cyclones in this region, and a detailed list is given in the Database of Cyclonic Storms in Bangladesh, West Bengal, and Odisha for the period 1877–2016 (Bandyopadhyay et al., 2018; or <https://datacatalog.worldbank.org/dataset/cyclone-dataset>), showing more than 170 cyclones making landfall since 1877. A number of these have caused deaths in the tens and hundreds of thousands, with Cyclone Nargis in 2008 perhaps being the most recent (Fritz et al., 2009).

Super cyclones, defined as storms with sustained winds of over 220 km/h, are multi-hazard events. During these events, it is often the storm surge flood inundation that leads to the majority of deaths, sometimes accounting for up to 80% of the total mortality (Shultz et al., 2005). In Bangladesh, for instance, it is the storm surge-induced flood inundation that is by far the most dangerous impact of a cyclone for human life (Chowdhury et al., 1992; Lin et al., 2012; Shultz et al., 2020). However, damages extend to significant losses to agriculture, finance, and long pauses in economic growth (Islam & Peterson, 2009). Despite the high societal risks, cyclones in this area have received significantly less attention than those in other cyclone basins (e.g. the IPCC Special Report on 1.5°C; Hoegh-Guldberg et al., 2018), with examples in those basins including Lin et al. (2012, 2016), Lin and Emanuel (2016), Patricola and Wehner (2018), and Vosper et al. (2020). The studies that do exist show that storm surge-induced population exposure from climate change is a serious issue for India, Bangladesh, and Myanmar, with all

three being among the 10 most exposed coastlines to storm surges in the world (Rahman et al., 2019). Notably, other countries in the top 10 have considerably higher GDP, and thus potential for resilient infrastructure (Nicholls et al., 2008; Dasgupta et al., 2011).

In the Bay of Bengal, the seasonality of cyclogenesis is more complex than other cyclone basins, and does not follow the summer increase in sea surface temperatures as one might expect. While the increase in sea surface temperatures is still a key factor for cyclones forming in the region (Krishna, 2009), the cyclogenesis is bimodal in time, with maxima in both early to mid-summer (April–May) due to increased relative humidity fuelling storm formation, and in autumn (October–November) due to decreased vertical wind shear not shearing the storm apart (Yanase et al., 2012; Li et al., 2013). Throughout the rainy season (June–August), the cyclogenesis is significantly impeded by strong vertical wind shears, amongst other factors such as local vorticity (Yanase et al., 2012). This additional complexity further reinforces the need for more research into cyclones occurring in this region, to increase understanding of present-day cyclones both in terms of their dynamics as well as their impacts, which may vary depending on the month that the cyclone occurs, particularly in the case of agricultural impacts.

Damages from cyclones that make landfall are multifaceted, being a product of the physical climate system (i.e. the cyclone), on the one hand, and socio-economic and behavioural patterns on the other (Shultz et al., 2005). Access to good quality forecasts, disaster response training, and resilient storm shelters are essential to reduce the vulnerability to storm surge, and many of the poorer households along the coast of South Asia do not have these advantages (Bern et al., 1993; Fritz et al., 2009; Hossain, 2015). For example, the cost of forecasting centres working together to provide better cyclone lead times is orders of magnitude lower than the costs of damages associated with these cyclones on unprepared populations. This point was argued clearly when comparing the mortality counts

of intense tropical cyclones hitting the east coast of America, against those hitting Bangladesh and Myanmar (Webster, 2013). For adaptation measures to be put in place at the national level, the costs can easily reach several percent of a country's GDP, and this is certainly true for India and Bangladesh (Anguelovski et al., 2016; Oppenheimer et al., 2019). A number of studies have shown that future increased risk from tropical cyclone flooding is dominated by sea level rise (SLR), allowing the storm surge to reach further inland (Knutson et al., 2010, 2020; Woodruff et al., 2013; Lin et al., 2016), with Dastagir (2015) providing an overview specifically of Bangladesh. For instance, even under moderate SLR (~ 0.25 m) resilience investment would cost Bangladesh more than \$2.5 billion, with ongoing costs of \sim \$50 million annually (Dasgupta et al., 2014). The problem is not one that can be solved entirely with adequate finance, and Bangladesh in particular has clear examples of low-exposure land being taken by powerful groups, leaving the more exposed regions to those least able to adapt (Sovacool, 2018; Oppenheimer et al., 2019).

Behavioural responses to cyclones add a layer of complexity onto an already complex physical science problem. While there are consistent messages that globally the most intense tropical cyclones will increase in frequency under climate change (Walsh et al., 2019; Knutson et al., 2020), less confidence is obtained at the basin level. For the satellite era, studies in the North Indian Ocean are somewhat contradictory, with cyclone energy-based metrics showing an increase in the most intense storms (Yu & Wang, 2009; Balaji et al., 2018), but cyclone count-based metrics showing a decrease (Mohapatra et al., 2017). Attributing the characteristics of any 'specific' cyclone event to particular causes is extremely difficult, while at the same time such 'extreme event attribution' methodologies have been very insightful for different types of extreme weather event (NAS, 2016). Certainly, no such event attribution study exists for the Bay of Bengal basin. Although there have been some studies focussing on the Atlantic basin, due to the complex nature of cyclones, they have concentrated on the meteorological response, namely precipitation (Emanuel, 2017; Risser & Wehner, 2017; Van Oldenborgh et al., 2017) or wind speed (Patricola & Wehner, 2018), rather than the hazard response. However, two examples of attribution of the hazards are Lin et al. (2016) and Wehner and Sampson (2021). Lin et al. (2016), showed that the return period for Hurricane Sandy's flood height in New York would decrease by ~ 4.4 times, from 2000 to 2100, under a moderate-emission scenario. Wehner and Sampson (2021) showed that the attributable increase in flood area was lower than the attributable increase in precipitation alone. Here, we consider the storm surge-induced flood hazard, applied to the Bay of Bengal Super Cyclone Amphan. We also consider the change in exposure

of the populations in its path. Specifically, our main aim is to 'understand how population exposure to an Amphan-scale storm surge would change with different future levels of SLR', and in doing so we have the following sub-aims:

1. To focus specifically on a single tropical cyclone, Amphan, in order to understand the narrative of that event in the present and future, while at the same time recognizing that different tropical cyclones making landfall on the Indo-Bangladesh shoreline may have different impacts.
2. To study a recent event, which is not too extreme, highlighting how even the impacts of events of this scale can become 'extreme' under a changing climate.
3. To isolate the exposure purely from climate change or population change within the region, rather than from future adaptive or other socioeconomic changes, thus highlighting the potential impact if relevant decisions are not made ahead of time.

2 | METHODS

2.1 | Cyclone Amphan damage data

Secondary data for the emergency response to Super Cyclone Amphan, the damage estimates, and the reports of interplay with COVID19 were obtained from situation reports by several NGOs (namely the Red Cross/Red Crescent, and Climate Central), and supplemented by some Bangladeshi governmental departments, including the Department for Disaster Risk Reduction. The data were collected in the days following the cyclone impact using surveys (called D forms) by NGO teams in the field, and sent to a central team. These teams collated the data and combined it with assessments from satellite images of the affected areas. Most of these data are only available for Bangladesh; however, as the cyclone also hit parts of India, the expected damage will also be high there. Myanmar was less impacted by this particular cyclone.

2.2 | Climate model projections

For the global mean temperature and SLR calculations, we use models from the Coupled Model Intercomparison Project (CMIP6) (Eyring et al., 2016). For global mean temperature calculations, we adopt the IPCC Special Report on 1.5°C definition of the Paris Agreement climate goals (Allen et al., 2018), which defines 'pre-industrial' as the average period from 1850 to 1900, and considers a global mean temperature increase of 1.5 and 2°C relative to that.

To calculate the global mean temperature, we use area-weighted ‘temperature of air at the surface (tas)’ from each of the models. We use three separate future scenarios, as prescribed in the CMIP6 models as low emission (SSP1-RCP2.6), business-as-usual (SSP2-RCP4.5), and high emission (SSP5-RCP8.5). The Shared Socio-economic Pathway (SSP) label in each scenario gives information about the change in socioeconomics, including population (see Section 2.5), and the RCPs (Representative Concentration Pathways) give the radiative forcing scenario, which represents, for example, an increase of 2.6 W/m^2 by 2100 for the RCP2.6 case.

The projections of SLR over the period 2020–2100 were obtained from the same CMIP6 experiments, but also included other published values and datasets. As the CMIP6 climate models have oceans that conserve volume rather than mass (the so-called Boussinesq-approximation), their sea level does not reflect net steric expansion (Greatbatch, 1994). Therefore, global mean steric height was calculated for each available SSP-RCP model run by computing density from the potential temperature and salinity fields, vertically integrating the density anomaly (relative to the mean density) to obtain two-dimensional steric height fields, and finally integrating over the ocean surface to obtain timeseries of global mean steric expansion. This was then added to the corresponding dynamic sea level and the annual means for 2020 and 2100 were calculated.

Corresponding estimates of SLR due to mass input were obtained from Oppenheimer et al. (2019) (see their table 4.4). The mass contributions to global mean SLR for RCPs 2.6, 4.5, and 8.5 were obtained simply by subtracting the given steric contributions (based on CMIP5 models) from the total SLR for each RCP. A further 3.5 cm—as per a 25-year accumulation of the observed 1.4 mm/year rate of SLR due to mass flux, as given in Oppenheimer et al. (2019) (see their table 4.1)—was subtracted to adjust the SLR values to the 2020–2100 period required for this study. The final values obtained for RCPs 2.6, 4.5, and 8.5 were 0.22, 0.27, and 0.41 m, respectively. These were then added to the SLR maps for the corresponding SSP-RCP runs.

The SLR for the Bay of Bengal for each model run was obtained by computing the area mean over the region ($10\text{--}24^\circ \text{N}$, $78\text{--}98^\circ \text{E}$) for each map. The values obtained were adjusted to account for the regional relative sea level variations due to Glacial Isostatic Adjustment (GIA) and the gravitational influence of the ice-sheets. GIA was obtained from the ICE-6G_C model (Peltier et al., 2015), averaged over the Bay of Bengal to give a small drop in relative sea level (uplift) of 1.4 cm between 2020 and 2100. In determining regional variations in sea level due to the gravitational influence of ice sheets, glaciers, and other bodies of water, only fingerprints associated with Greenland

and Antarctica ice sheets were considered. According to sea level fingerprints in the Bay of Bengal (Milne et al., 2009; Church et al., 2013), gravitational effects will amplify the global mean SLR from the Greenland and the Antarctic ice sheets by approximately 20% and 10%, respectively. Using the Greenland and Antarctic contributions provided by Oppenheimer et al. (2019) (see their table 4.4), this will result in an additional SLR in the Bay of Bengal of 1.8, 2.2, and 3.6 cm for RCPs 2.6, 4.5, and 8.5, respectively. Since Church et al. (2013) (see their figure 13.17) suggest a small ($<1 \text{ cm}$) fall in sea level due to increased atmospheric loading (the inverted-barometer response) over the Bay of Bengal, and it is not possible to accurately estimate vertical land motion due to subsidence, these processes were not included in the analysis. For each future scenario, to avoid bias in cases where there are multiple realizations of a particular model, these are combined to form a mean SLR value for the Bay of Bengal (or SLR map) for that model.

2.3 | Flood inundation modelling

To model the storm surge-induced inundation from Cyclone Amphan, forecasts of water height along the coastline were taken from a high-resolution tide-surge model implemented on an unstructured grid over the Northern Bay of Bengal and passed as boundary conditions to a hydrodynamic model to simulate inland flooding. This approach was chosen to allow a detailed, spatially variable set of time-varying water heights to be passed to the hydrodynamic model.

The tide-surge model is based on SCHISM-WWM (Zhang et al., 2016) and is online coupled with a spectral wave model to account for the wave setup over the nearshore region. We have used FES2012 (Carrère et al., 2013) tidal water level to force our model at the ocean boundary and climatological discharges at the river boundaries. The atmospheric forcing for Cyclone Amphan is derived from a combination of the JTWC best-track estimate and the NOAA HWRf forecast using published analytical formulae for the wind (Emanuel & Rotunno, 2011) and pressure fields (Holland, 1980). Our model is solved at 5-min timesteps while updating the wave field every 30 min. Finally, simulated water heights are extracted at 30-min intervals along the coastline and provided as boundary conditions for the Fathom flood inundation model (Sampson et al., 2015).

The Fathom flood model is a two-dimensional hydrodynamic model based on the LISFLOOD-FP numerical scheme. It solves a local inertia approximation of the Shallow Water equations (Bates et al., 2010; de Almeida & Bates, 2013) over a 3-arcsecond ($\sim 90 \text{ m}$) spatial resolution regular grid, with river channels treated as variable-width

sub-grid scale features in one dimension. The model has been applied in a simplified manner to this site previously (Lewis et al., 2013) and in a range of modelling studies since, including to simulate tropical cyclones (Wing et al., 2019). The Digital Elevation Model (DEM) that provides terrain elevations to the hydrodynamic model is obtained from MERIT-DEM, a 3-arcsecond global terrain dataset that is the most accurate freely available global terrain dataset for flood modelling (Yamazaki et al., 2017). MERIT-DEM combines elevation data from several sources (SRTM, ASTER, ICESat), which are then processed to remove vegetation, stripe noise, random noise, and absolute biases. It has been proven to resolve many errors in flat floodplains (like those in the Bay of Bengal) that are present in other satellite-based terrain datasets (Yamazaki et al., 2017). The DEM has been processed further to correct for urban developments by applying a filter based on a remotely sensed global urban footprint dataset to remove data at cells classified as urban in areas of low gradient. Corrected elevations at these locations are then interpolated from the remaining neighbouring elevation data.

The hydrodynamic model takes the modelled water heights from the storm surge model, linearly combined with future climate-induced perturbations, and applies these as a height-varying boundary condition across its coastline. The simulations were performed at the native spatial resolution of MERIT-DEM (3 arcsecond). The height and location of flood defence polders in Bangladesh were provided by the Bangladesh Water Development Board. The heights of the polders were converted from Public Works Datum to mean sea level and burnt into the DEM of the hydrodynamic model. Flood defence data were not available in India so have not been included. Maximum water depths from the hydrodynamic model are computed across all cells over the course of the simulation to undertake exposure analyses. As the hydrodynamic model simulates water heights, the model will be sensitive to both the size of a storm surge and with how the time of the peak storm surge coincides with the phase of the tide.

One of the uncertainties in modelling flood inundations is the choice of terrain data that is used to build the DEM that defines the ground elevations. This is especially the case when building large-scale models in locations with limited local data available to supplement global datasets, particularly in locations where geomorphological processes cause ground elevations to change over time, for example through coastal erosion or land subsidence. The DEM used here, MERIT, is a derivative of SRTM that has multiple error sources reduced (e.g. the removal of striping, noise, and errors from vegetation). This results in significant improvements upon the raw SRTM data, with approximately 50% of flat unvegetated areas (slope less than 10%) having a vertical error of less than 1 m and 72%

less than 2 m. Errors are also shown to be small within our study area (Figure 2c in Yamazaki et al 2017). Furthermore, Hawker et al. (2019) also found MERIT-DEM to have mean errors of approximately 1 m when assessing performance across multiple flat locations (like those in this study). Since these studies, we have made further improvements to the MERIT-DEM by incorporating the elevations of Polders in Bangladesh to ensure that these flood defences are correctly accounted for in the hydrodynamic simulations. We also considered using another global DEM (CoastalDEM, Kulp & Strauss, 2019), but found CoastalDEM to be noisy and have striping artifacts in our study site which is not conducive to flood simulations (see Figure S3).

2.4 | Hydrodynamic model validation

The hydrodynamic model used in this study (LISFLOOD-FP) has previously been validated in being able to replicate several physically based test cases (de Almeida & Bates, 2013). However, validating the modelled flood extents for this event is difficult due to the limited observations of flood extent that can be directly attributed to the storm surge. This is primarily due to the timing and noise present in satellite overpasses and uncertainty in field observations. For example, imagery from Sentinel-1 is only available for 22 May 2020, 2 days after the Cyclone made landfall. This means that not only will the peak inundation caused by the storm surge have been missed due to the delay between the peak storm surge and satellite overpass, but that there are likely to be significant amounts of surface water flooding caused by excess rainfall and not by the storm surge that are detected in the Sentinel-1 image. This is especially the case given that the rate of rainfall was in the range of 50–60 mm/h across many districts in the West Bengal region, including a cumulative daily total of 650 mm over Purba Medinipur on 20th May (Michra & Vanganuru, 2020). In addition to this, many areas will be either permanently or seasonally flooded, whilst the presence of mangroves such as those in the Sundarbans can inhibit the ability of satellites to detect water on the surface.

Given the above, we have compared our model to two data sources. The first is a processed version of Sentinel-1 produced using the *siflood* algorithm described in DeVries et al. (2020). Surface water is classified into several categories—flood, seasonal inundation, and permanent water. It is important to note that the classification scheme does not distinguish between the process that caused flooding, so we cannot distinguish if flooding was caused by coastal flooding, riverine flooding, or excess rainfall. Unfortunately, as the Sentinel overpass was

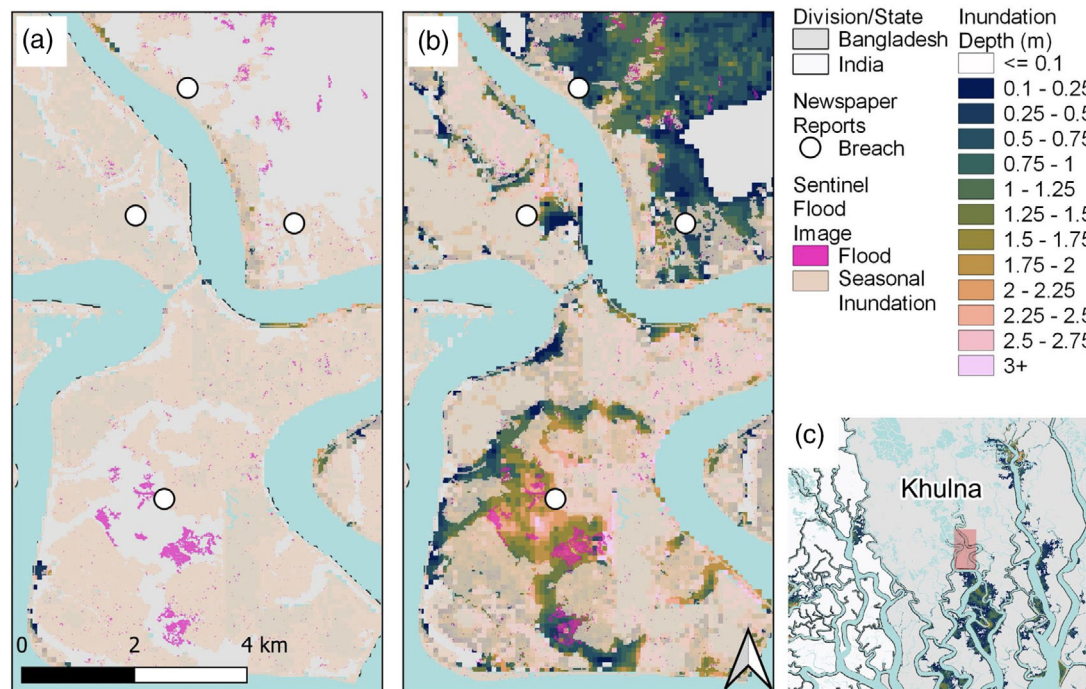


FIGURE 1 Comparison of defended to undefended hydrodynamic model for a selected area in Khulna, Bangladesh. Panel (a) shows the defended model, with observations from Sentinel (pink) and reported breaches (white dots). Modelled inundation (dark blue to light pink) is minimal due to the presence of polders. Panel (b) shows the undefended version of the hydrodynamic model. Modelled inundation matches correspond more closely with the observation data. Panel (c) shows an inset map. Beige represents seasonal inundation as classified by the s1flood (deVries et al., 2020) tool

~2 days after landfall only the remnants of coastal flooding are likely to be captured, and thus we would expect to see a much smaller inundation extent recorded by Sentinel.

The second observational data source is geotagged reports of flooding from local Bengal Delta newspapers (Khan, 2020). In total, 88 locations were digitized, with a flooding mechanism of breaching, overtopping, or high-tide assigned to each. The news reports of dike breaches in India were not deemed of satisfactory quality by Khan (2020), so the reports are limited to Bangladesh. This dataset has the benefit of being more directly comparable to the storm surge model as most reports are on the day of landfall or the day after. However, the dataset does have limited geographic coverage and does not give inundation extent. Moreover, the geolocation of reports is likely to be subject to uncertainty and their accuracy may not be commensurate with the resolution of Sentinel 1 (~10 m) and the hydrodynamic model (~90 m)

In areas in Bangladesh, the hydrodynamic matches reasonably with the Sentinel imagery, albeit with a smaller extent. Visualizing a comparison of the entire region is difficult given the fine-scaled nature of flood inundation, but a representative region is given in Figure 1b. As expected, the Sentinel flooding has a smaller extent than the model due to the coastal flooding receding. In general, however, for this region and other regions of Bangladesh (not

shown) we see reasonable agreement between the two observational data sources, and the modelled flood extent, especially given the limitations noted above. Areas where the model performs less favourably are in West Bengal, India which is most likely due to the absence of Indian polders in the model, but also possibly the coastal flooding receding by the time of the satellite overpass. Moreover, in the Sundarbans, the hydrodynamic model shows flooding in this region, but the SAR-based Sentinel imagery does not due to difficulty in characterizing the appropriate backscatter for flooding in vegetation (and indeed heavily built-up areas) (DeVries et al., 2020; Singha et al., 2020).

The newspaper dataset identified some of the polders that were breached during the storm surge. However, these breaches would not be included within our defended model and therefore we would not expect the defended model to show flooding in these locations. As the exact number, location, and size of the breaches are not known, we have run an undefended model without polders to capture this unknown within our modelling (Figure 1). We compare the defended model (Figure 1a), with the undefended model (Figure 1b) for an area in Khulna, Bangladesh. We overlay the Sentinel-derived flood extent, as well as locations of reported breaches. In the defended model, modelled flooding is limited and is less than the Sentinel-derived flood extents. However, in the

undefended model, the model flood extents compare more favourably to the Sentinel imagery, with the largest areas of flooding occurring at reported breach points.

Both sources of flood observation are subject to large uncertainties, but are the best available to aid in validating the hydrodynamic model. As noted before, the observational data and modelled data do not necessarily show the same thing (i.e. coastal flooding) at the same time (i.e. the satellite observations are ~2 days after landfall), thus a stringent validation is not possible. However, it does allow for a qualitative comparison, especially given our understanding of the events as they unfolded. This, combined with the previous validation studies of the model, gives us confidence that our flood inundation modelling is capturing the relevant processes for this event, in the relevant locations, at least within the uncertainties addressed previously.

2.5 | Exposure response

The number of people exposed to flooding (hereafter referred to as flood exposure) is calculated by overlaying the projected flooded area on a gridded population dataset. In this study, we use the High-Resolution Population Density Map (HRPDM) at 1 arcsecond resolution (~30 m) available at the Humanitarian Data Exchange (Facebook Connectivity Lab, 2016). HRPDM is a follow-up of the High-Resolution Settlement Layer (HRSL) project and currently covers most countries. We chose to use HRPDM as it has been demonstrated that other coarser resolution gridded population products tend to overestimate flood exposure compared to HRSL, especially in rural areas (Smith et al., 2019). This is due to a low-density spreading of population in rural areas in data sets other than HRDPM. Population is then aggregated to 3 arcsecond (~90 m) to be commensurate with the resolution of the flood inundation data.

To calculate future flood exposure, gridded population projections are required. To be consistent with our climate emission scenarios, we use the CMIP6 Shared Socioeconomic Pathways (SSP) population and urbanization projections, available at country level (IISA; Jiang & O'Neill, 2017; Riahi et al., 2017; Samir & Lutz, 2017). The SSP scenarios are not gridded. Gridded population projections for India and Bangladesh exist at resolutions of ~13 km (Jones & O'Neil, 2016) and ~1 km (Merkens et al., 2016; Gao, 2017). Calculating flood exposure using gridded population data at the kilometre scale is likely to lead to significant overestimation (Smith et al., 2019). Furthermore, the aforementioned gridded population projection products unrealistically spread population in rural areas which leads to further overestimation as noted above. Therefore, to create a more plausible estimate of population projec-

tions that is commensurate with our flood hazard data, we use the methods of Boke-Olen et al. (2017) to produce population projections at 3 arcsecond (~90 m) resolution for 2100 based on the SSP and RCP combinations highlighted earlier (SSP1 RCP2.6; SSP2 RCP4.5; SSP5 RCP 8.5) and the HRPDM population data for 5 Bangladeshi Divisions (Barisal, Chittagong, Dhaka, Khulna, and Rajshahi) and 2 Indian States (Odisha and West Bengal). The premise of this method is to distribute country SSP population and urbanization rates from the SSP Public Database (IIASA, 2018) onto the 3 arcsecond aggregated population grid based on a 0.25° RCP-specific urban fraction grid and a ranking of pixels into urban/rural based on distance to roads and population centres of gravity. First, water bodies were removed from the HRPDM population data using the G3WBM water mask (Yamazaki et al., 2015). Urban/rural classification of the 3-s pixels was implemented by adding rescaled inverse distance to roads and inverse distance to population centre of gravity (COG) to the HRPDM data to create a 'unique population' layer. Inverse distance to roads is the Euclidean distance to roads on OpenStreetMap, and the population COG is calculated using the COGravity tool from the SDMTools package in R. The RCP urban fraction data (version LUH2 v2f; Hurtt et al., 2020) provide the proportion of urban land at a 0.25° (~25 km) resolution between 2015 and 2100 for each RCP scenario based on CMIP6, and is subsequently leveraged to classify urban/rural pixels. For each 0.25° urban fraction cell, the 3-arcsecond pixels of the unique population layer (i.e. HRPDM+inverse distance to COG+inverse distance to roads) are ranked, with the highest value having the highest ranking. An urban mask is created by selecting the highest percent of pixels that correspond to the urban fraction in each 0.25° cell. Subsequently, the urban population by Division/State per SSP is allocated to urban pixels, while the rural population is distributed to rural pixels. The country-level SSP population estimates were disaggregated to the Division/State level by weighting the proportion of each Division/State population compared to the national population based on the most recent census for both countries (2011 in both cases). Whilst this does not capture the heterogeneity of population projections and urbanization rates within countries, it does allow for population projections at the sub-national scale. SSP urbanization rates were assumed to be identical across all states per country. Projected population gridding is calculated recursively with the previous year's population being used to create the urban mask for the following year. To this end, we generate gridded projected population at 3 arcsecond resolution (~90 m) every year between 2018 and 2100 for the seven administrative regions assessed in this study.

Flood exposure is then calculated by performing pixel-wise raster multiplication using the population data and

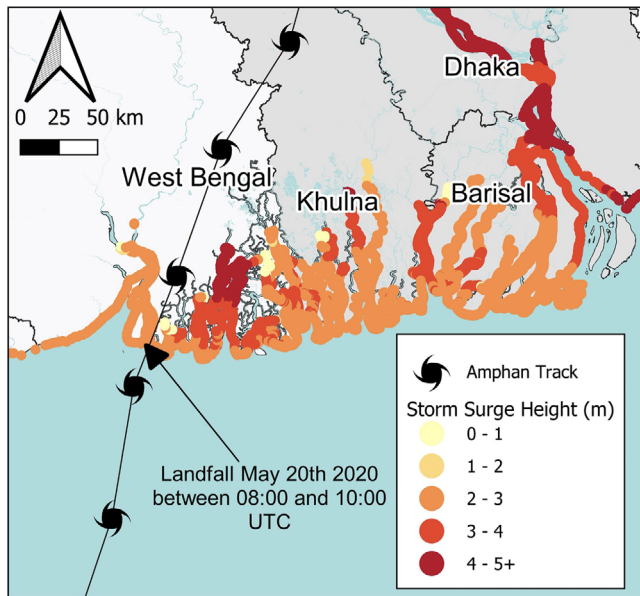


FIGURE 2 The centre of the storm track of super cyclone Amphan over the Bay of Bengal, India (white) and Bangladesh (grey). The maximum storm surge height above sea level at the coast during the time of landfall is coloured according to the legend. The storm location and timing are from the International Best Track Archive for Climate Stewardship (IBTrACS). For the storm surge height data, see Section 2

inundation maps converted to binary (where 1 = wet; 0 = dry). We use three severity levels to generate the binary inundations maps (low = >0.1 m; medium = >1 m; high = >3 m) based on the flood water depth. Exposure raster maps are subsequently produced at 3 arcsecond (~ 90 m) resolution. Lastly, exposure statistics per administrative unit were performed using zonal statistics and administrative units from GADM (GADM, 2020).

3 | RESULTS

Super Cyclone Amphan made landfall on the India-Bangladesh border on the 20th May 2020 (Figure 2). It was the strongest cyclone in the region since 1999, with 1-minute sustained wind speeds of up to 72 m/s at its peak (category 5 on the Saffir-Simpson scale). However, a significant wind deceleration to around 43 m/s (category 2) was observed at the time of landfall. Even so, our modelling indicates that most of the coastal regions of India and Bangladesh experienced a storm surge of 2–4 m around the time of landfall, which occurred during the ebb tide period (see figure 5 in Khan et al., 2021), with storm surge heights reaching up to 5 m on parts of the River Ganges, for example near Dhaka (Figure 2). Our modelling indicates that this level of storm surge would lead to exposure of around 737,000 people in Bangladesh and 420,000 in India

from the ensuing flood inundation (Figure 3). In the most extreme populated regions, especially in Bangladesh, 2–2.5 m of flooding is estimated, bringing saline water to settlements and agricultural land. Even with some larger urban regions that are more inland, such as the administrative region of Dhaka, flooding of >0.1 m exposed 1%–3% of the population in some Districts (Figure 3b). Given the high population density, we see exposures of up to 140,000 in the Dhaka Division, rising higher in more coastal areas, such as West Bengal, where $\sim 400,000$ people were exposed.

The human mortality estimates for the days surrounding Cyclone Amphan landfall were considerably lower than for other similarly intense cyclones in the region, ranging between 100 and 200 deaths according to the situation reports (see Section 2) and local media broadcasts. While the total attributable mortality is often found to be higher when longer term effects are considered, such as disease and infection from contaminated water, or specifically to Cyclone Amphan, the disruption due to the ongoing COVID-19 pandemic protocols (Shultz et al., 2020), the mortality will still likely be substantially lower relative to previous super cyclones in the region. This is likely attributed in part to increased preparation time, with over 48 hours' notice of the landfall site from five different forecasting systems which allowed for the evacuation of several million people, in addition to well-developed humanitarian response plans that have been established in recent years. Examples of these include the Early Action Protocols setup by NGOs such as Climate Central and the German Red Cross, which have been adapted for Bangladesh by the Needs Assessment Working Group (NAWG), a Bangladeshi governmental body. Nevertheless, other societal damages from the cyclone were on par with, and in many cases greater than, previous super cyclones in the region, namely from commodities that are immovable. For instance, in Bangladesh, according to data collected from regional surveys (see Section 2), it is estimated that there were hundreds of thousands of cattle lost, tens of thousands of buildings destroyed, and $\sim \$20$ million worth of damage to fisheries alone, primarily from the storm surge. During the month of May, fisheries are the primary source of agricultural income for the region, and damages to other agricultural sectors, such as rice paddies and mango crops, totalled a factor of 4 smaller than that.

3.1 | A changing earth system

With principal damage from intense cyclones predominantly coming from the storm surge (Shultz et al., 2005), we concentrate here on how this impact of the cyclone would change under a range of future climate scenarios associated with a range of carbon emissions,

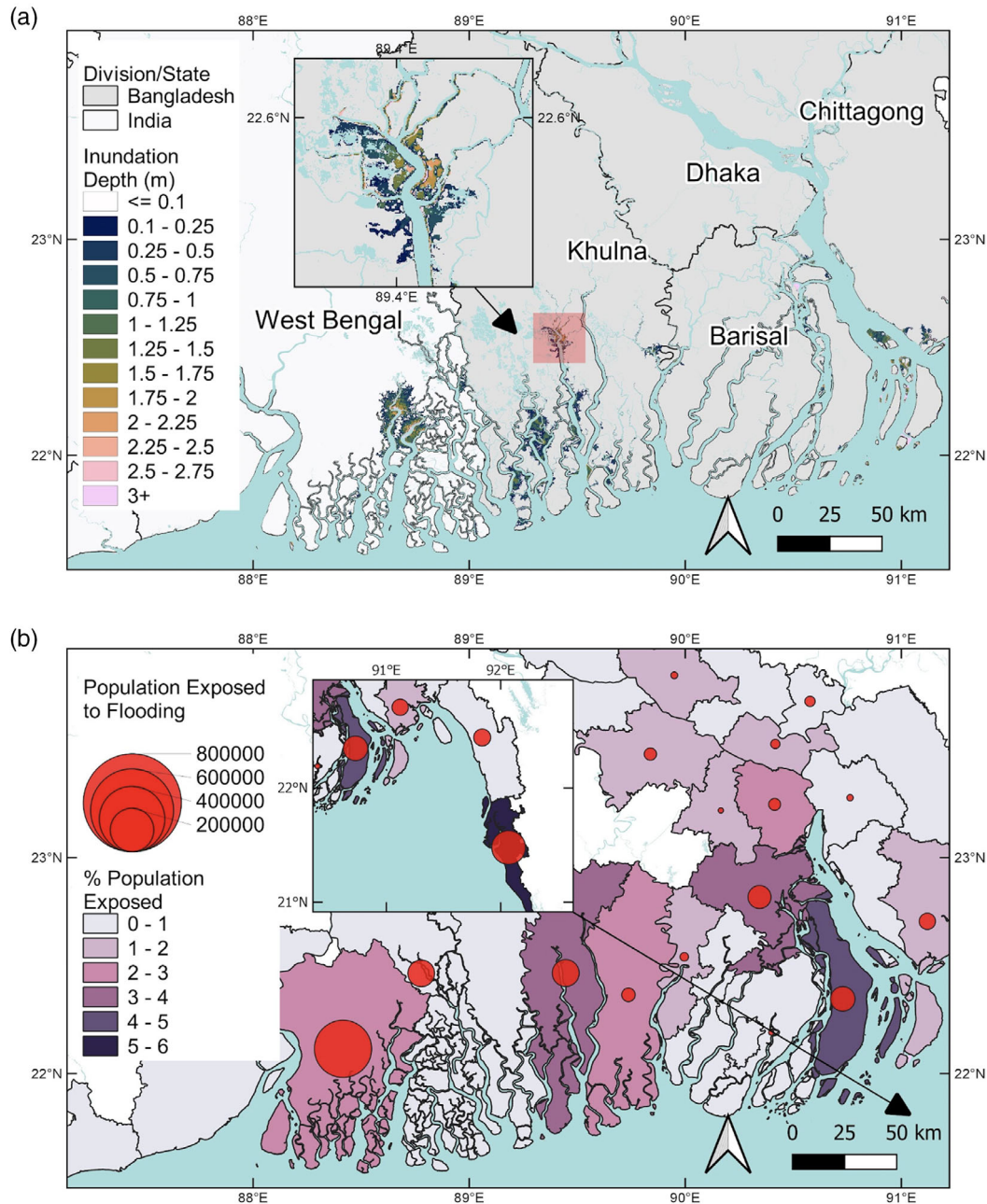


FIGURE 3 Flood inundation and exposure maps of Super Cyclone Amphan landfall. Both maps show the Indo–Bangladesh border and surrounding regions. Panel (a) shows the modelled storm surge flood depth in meters on the 20th May 2020. Inundation depth is particularly hard to see on a map of this scale as it manifests much more locally, so a zoomed segment is also given as an example. Administrative regions are named. Panel (b) shows the population exposed to flooding, as a percentage of the total regional population (pinks) and as absolute numbers (red circles), defined as areas with a flood depth greater than 0.1 m on the 20th of May 2020. The size of the red circles is proportional to the number of people exposed, as displayed in the figure key

thereby giving an assessment of future vulnerability in this region. Specifically, we consider the change in future SLR, as predicted by the Coupled Model Intercomparison Project, phase 6 (CMIP6; Eyring et al., 2016). We analyse three future scenarios spanning a low-emission scenario (SSP1-RCP2.6), a business-as-usual scenario (SSP2-RCP4.5), and a high-emission scenario (SSP5-RCP8.5), (see Methods for further information). Climate

models run under the low-emission scenario indicate, on average, a 2°C global mean temperature increase by 2100 since pre-industrial (Figure 4a), defined as 1850–1900 (Allen et al., 2018). We therefore consider this as a proxy-scenario for the upper goal of the Paris Agreement (Allen et al., 2018), with the other scenarios reaching around 3°C and 5°C, therefore exceeding the Paris Agreement goals.

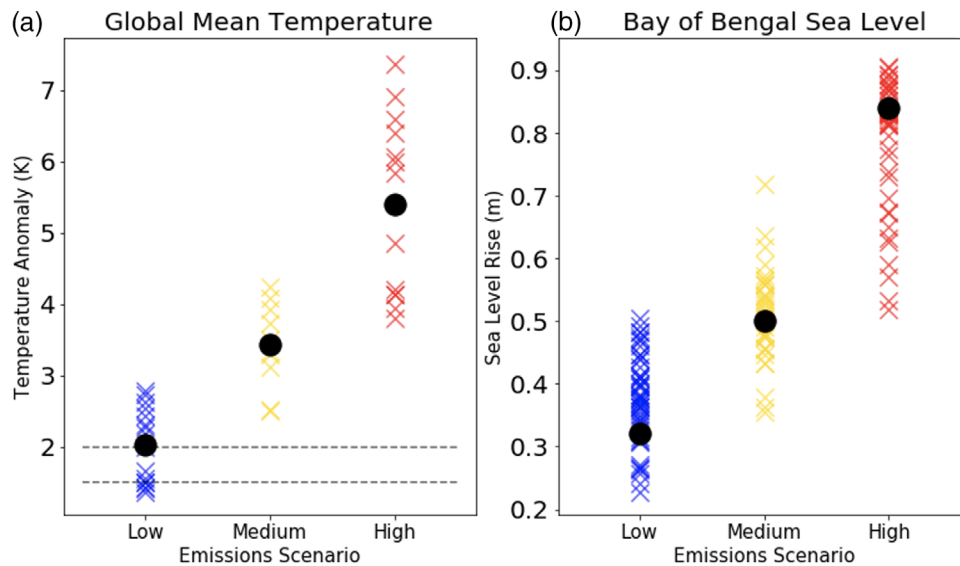


FIGURE 4 Global mean temperature, and sea level rise projections in the Bay of Bengal. (a) Global mean surface temperature increase for the decadal average of 2090–2100, compared with pre-industrial (1850–1900). Each coloured cross shows the first ensemble member of a CMIP6 model (see Section 2). Black circles show the multi-model mean, and dashed lines show the Paris Agreement climate goals. (b) Individual crosses show the area-averaged sea level height for the Bay of Bengal (10N–24N) for each of the individual models and ensemble members used, in the month of May. Black circles show the lower quartile value for the blue crosses, mean value for the yellow crosses, and upper quartile value for the red crosses. The values are anomalies between 2020 and 2100

Focussing now on how these temperature scenarios relate to SLR, we consider the multi-model mean SLR projections from the business-as-usual scenario; the multi-model lower quartile sea-level rise from the low-emission scenario; and the multi-model upper quartile response from the high-emission scenario, giving a range in sea level responses over the region (Figure 4b). The results are targeted for the month of May and only for the Bay of Bengal (10–24N), and indicate that there will be 0.32, 0.50, or 0.84 m of SLR between the Cyclone Amphan event (2020), and the end of the century (2100), for our low, medium, and high scenarios, respectively.

3.2 | Projected storm surge exposure

Given that the entire range in predicted SLR is positive, we know, all other factors remaining constant, that the exposure in South Asia from cyclone storm surges will also increase. However, we must also consider future population change: not only the projected increase in population for India and Bangladesh, but also the migration of populations, which, for this region, manifests as a significant shift from rural to urban settlements (Figure S1). Under the SSP5 scenario, for example, the percentage of the population living in urban areas is projected to increase from ~35% at present day to ~90% by 2100. Combining the SLR, storm surge modelling, and changes in population (see Section 2), we see significant

increases in population exposure, especially in India (Figure 5).

An informative way of interpreting the storm surge exposure is by considering different severity levels of flood depth, and it is common practice to consider low (>0.1 m), medium (>1 m), and high (>3 m) flooding. There is a clear positive increase in future exposure for all severity levels under most future scenarios, except for the low-emission scenario in Bangladesh (Figure 6). The reasons for this decrease are discussed later. The largest increases in exposure are estimated in India, with flooding increasing by 50%–90% even in the low-emission scenario, and reaching over 200% in the high-emission scenario (Figure 5c). The exposure changes in Bangladesh are considerably lower for all flooding severity levels, in general showing no change for the low-emission scenario, but ranging from around 50% to 80% in the high-emission scenario, depending on the flood severity level. It should be noted, however, that in terms of absolute numbers (rather than percentage change), Bangladesh sees a larger increase than India (Figure S2).

To test whether the exposure response is dominated by either climate change or population change, we also include a fourth scenario, where we use the high-emission projections but keep the population levels to those of 2020 (Figure 6d). We see that, for the least severe flooding (greater than 0.1 m), the exposure in India is nearly all from climate change, that is the yellow bars are of similar length in Figure 6c,d. For all other flood severity levels,

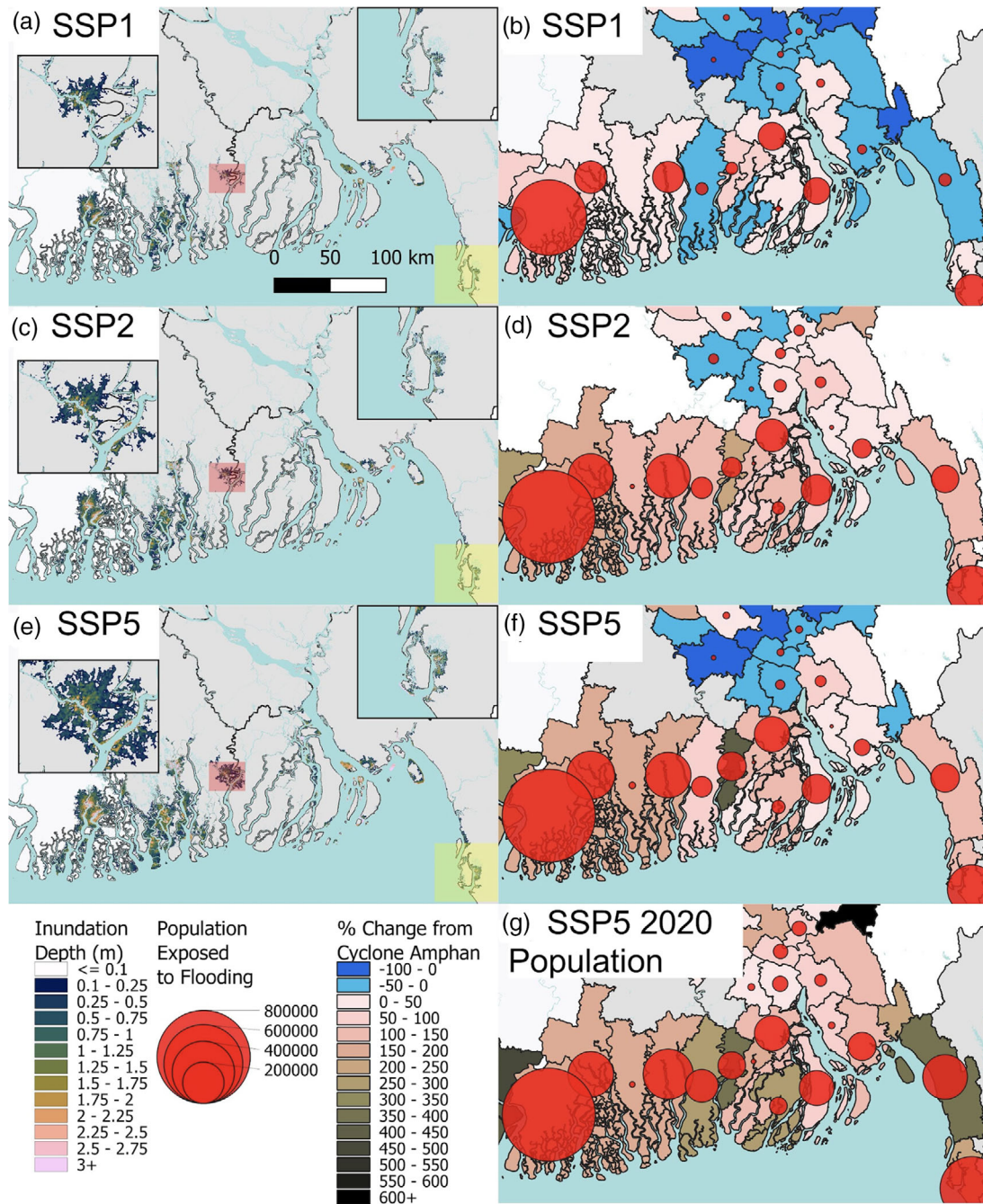


FIGURE 5 Projections of the flood inundation and exposure for Super Cyclone Amphan under different climate scenarios. Panels (a–f) are as in Figure 3, but for the three different sea level rise scenarios predicted for 2100. The blue and green colours now show the percentage change in exposure from the 2020 baseline. Panel (g) shows the same as panel (f), but keeping the population at 2020 levels

in both countries, the population changes negatively contribute to the overall exposure. The two primary reasons for this are (1) that communities are estimated to migrate from rural regions near the coast, to urban regions which are generally on higher ground, and (2) because population is projected to peak in 2050 in India and Bangladesh, before declining by varying degrees depending on the scenario used (see Figure S1).

3.3 | Discussion of societal impacts during Super Cyclone Amphan

Here, we have presented a physical mechanism for changes in exposures for a future Amphan-scale storm surge. But this is just one part of the physical and social system of impacts during tropical cyclones, albeit the most important for health (Shultz et al., 2005). A clear

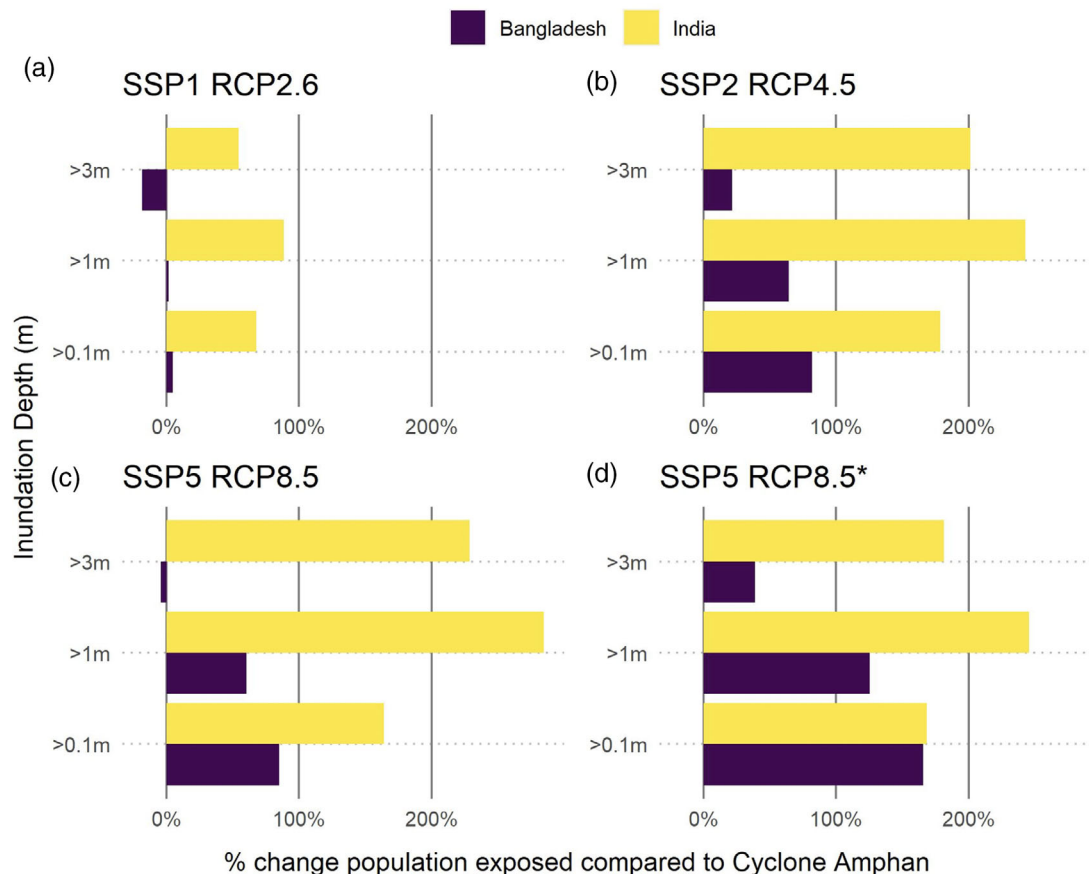


FIGURE 6 Projected changes in different levels of flood risk for India and Bangladesh. Bar charts of change in flood exposure for (yellow) India and (purple) Bangladesh measured in percentage change between the future (2100) and baseline (2020). For each country, three levels of flood severity are identified, corresponding to flood exposures of >0.1 m (low), >1 m (medium), and >3 m (high). The four panels represent four different future combinations of emissions and population change. Panel (a) shows a low-emission scenario, consistent with the upper Paris Agreement climate goal. Panels (b) and (c) show business-as-usual and high-emission scenarios, respectively. Panels (d) is the same as (c), but with 2020 populations. A version of this figure showing absolute changes, rather than relative changes, is given in Figure S2

example of compounding crises during this event was the interplay with the COVID-19 pandemic, where the potential for exacerbated damages due to compounded extreme climate is clear around the world (Phillips et al., 2020). Cyclone Amphan is an extreme example of how regional problems have been compounded by these two crises (Shultz et al., 2020). At this point, it is impossible to tell the attributable damage from Cyclone Amphan alone, because long-term health and economic impacts are yet to be realised, for example due to waterborne disease from contaminated flood water (Sehgal et al., 2002; Fredrick et al., 2015), dangerous heat exposure from the destruction of preventive cooling measures (Matthews et al., 2019), or the impacts of soil salinization on crop yields (Chen & Mueller, 2018). Yet, Cyclone Amphan has added complexity compared to 'typical' tropical cyclones. Setting aside the fact that it is harder to coordinate forecasting, emergency planning, and humanitarian relief efforts because of restrictions in place due to COVID-19, the lack of social dis-

tancing may well have prolonged viral transmission in the region.

For instance, according to situation reports when the cyclone hit (see Section 2), Bangladesh had around 4000 dedicated cyclone-resistant shelters, intended for evacuation of communities in particularly exposed regions. Under normal circumstances, these shelters would suffice. However, with social distancing restrictions in place due to COVID-19 the government funded an additional 9000 make-shift shelters, mainly through conversion of educational institutes and other public buildings. Other preventative measures were also put in place, such as providing COVID-19 health kits (face masks, soap, etc) to those in the shelters. However, even with the rapid implementation of these precautions, it may be that an increase in COVID-19 cases in the area occurs in the weeks following the cyclone.

As with any dangerous climate event, additional ongoing emergencies, such as COVID-19, along with the increased damages from the cyclone, put extra pressure

on infrastructure and resources, including, for example, relief aid and engaging willing volunteers to help shore up broken dams (Phillips et al., 2020). In the case of Super Cyclone Amphan, some facilities, such as hospitals, were not as overwhelmed as one might expect (see Section 2). This was due to the cyclone hitting rural settlements, where the hospitals did not have the equipment to treat COVID-19 patients anyway, and so had referred patients to larger urban hospitals further from the coastline.

4 | CONCLUSIONS AND FUTURE OUTLOOK

Despite being one of the world's most vulnerable regions to cyclone hazards (e.g. Nicholls et al., 2008; Dasgupta et al., 2011), countries surrounding the Bay of Bengal have received far less research attention than in many other cyclone-prone areas (Knutson et al., 2010; Emanuel, 2017; Risser & Wehner, 2017; Van Oldenborgh et al., 2017). This shortcoming must be addressed because countries of the region urgently need information on where best to enhance short-term emergency response plans, and where to focus longer term infrastructure resilience investment. For example, due to the lack of maintenance and funding, riverbank erosion, subsidence, and constant exposure to cyclones in recent years, many stretches of flood protection have failed around Bangladesh.

Here, we have set up a framework for assessing damages in terms of future population exposures to one of the most hazardous components of a cyclone, the storm surge. We consider how many additional people would be exposed to different levels of flooding, given a regional SLR ranging from 0.32 to 0.84 m, and specifically relate this to the Super Cyclone Amphan event, thereby addressing the question: 'If an Amphan-scale storm surge occurred under a world with increased sea levels, how might the population exposed change?'

Our key conclusions are that in high- and medium-emission scenarios, more than 200% people could be exposed to the most severe flooding in India, although the exposure increase is only between 0% and 20% in Bangladesh. For lower flood severity levels, between 160% and 280% more exposure is estimated in India, and 70%–90% in Bangladesh. Most of this change in exposure for both countries comes from increased SLR, rather than changes in population densities. If we consider a low-emission scenario consistent with the 2°C Paris Agreement climate goal, we see similar levels of exposure to the present day in Bangladesh, and significantly smaller increases in Indian exposure levels than estimated for the mid- and high-emission scenarios. While this result provides some very strong motivation to meet the Paris Agree-

ment climate goal, it must also be interpreted in the wider context of other cyclone-coincident hazards, for instance the occurrence of deadly heat following cyclone landfalls in South Asia is likely to increase by as much as 70% under a 2°C target (Matthews et al., 2019).

There are several caveats to our analysis. As with any climate event, Cyclone Amphan will, strictly speaking, remain a unique event in Earth's history. However, it is likely that cyclones with similar relevant features, or even more extreme features, will occur in the future. Therefore, conceptually it does make sense to think of how a "component" of that event might have impacted society differently, given some change in the background Earth system, an approach often used in the insurance industry and referred to as 'realistic disaster scenarios'. Our example therefore considers how a storm surge of 2–4 m, sitting on top of varying degrees of SLR, might impact different parts of South Asia. We also choose not to simulate any future upgrade of flood defences in our hydrological analysis, meaning that our future Super Cyclone Amphan exposure estimates will be an overprediction if such investments are in fact made. Again, conceptually this makes sense from an attribution point of view, as we are keen to understand the climate and population drivers, without confusing the picture regarding changing coastal protection measures. The largest uncertainty in our analysis comes from the uncertainties in our Digital Elevation Map (see Section 2.3), which is not as accurate as in countries that have LIDAR-derived elevation maps, and so decreases the confidence in our results. It is hard to validate the subsequent flood inundation because like-for-like observational comparisons do not exist, and to some extent the modelling provides our best guess at what actually happened. Given this, and considering the extreme nature of hydrometeorological hazards in Bangladesh, it is important to use these maps accepting the reduced confidence, rather than avoid the problem altogether (Kulp & Strauss, 2019).

Our work here highlights the particular vulnerabilities that India and Bangladesh will face for cyclone hazards in the future, and provides a compelling argument for world governments to limit carbon emissions to be consistent with the Paris Agreement climate goals (Mitchell et al., 2016). On a regional level, planning and communication of disaster risk reduction is key, and was likely a major saving grace for Cyclone Amphan. In the past, there have been examples of conflicting communities in Bangladesh who, when properly incentivized, work together to overcome coastal flooding hazards (Sultana & Thompson, 2017). It is initiatives like these that need to be at the forefront of the Bangladeshi and Indian government mitigation strategies, possibly championed by the Loss and Damage initiatives (Huq et al., 2013; James et al., 2014), and with contingency

plans in place to deal with these particularly extreme compounded events.

ACKNOWLEDGEMENTS

DM was supported by an NERC fellowship (NE/N014057/1) and NL by EMERGENCE (NE/S005242/1). All University of Bristol authors had partial funding from the GCRF CRISIS project. PB is supported by a Royal Society Wolfson Research Merit award. JUK, FD, and YK acknowledge financial support from CNES (through the TOSCA project BANDINO), Embassy of France in Bangladesh, and the French research agency (Agence Nationale de la Recherche; ANR) under the DELTA project (ANR-17-CE03-0001). This work was granted access to the HPC resources of IDRIS under the allocation 2020-A0070107298 made by GENCI. JN and LH are funded under NE/S003061/1 and NE/S006079/1. The modelled atmosphere and ocean data in this study are available through the CMIP6 archive. The DEM was modified using data from the Bangladesh Government. The storm surge data are available from FD's group. The flood inundation data are available from the FATHOM group.

DATA AVAILABILITY STATEMENT

All data presented in our analysis are available through the University of Bristol data archive. All code used for the analysis is available from the Bristol Climate Dynamics group GitHub: https://github.com/BrisClimate/Amphan_population_exposure.

ORCID

Dann Mitchell  <https://orcid.org/0000-0002-0117-3486>

Laurent Testut  <https://orcid.org/0000-0002-3969-2919>

REFERENCES

- Allen, M.R. et al. (2018) Framing and Context “in Global Warming of 1.5 C: An IPCC Special Report on the impacts of global warming of 1.5 C above pre-industrial levels and related global greenhouse gas emission pathways, in the context of strengthening the global response to the threat of climate change, sustainable development, and efforts to eradicate poverty.
- Angelovski, I., Shi, L., Chu, E., Gallagher, D., Goh, K., Lamb, Z., Reeve, K. & Teicher, H. (2016) Equity impacts of urban land use planning for climate adaptation: Critical perspectives from the global north and south. *Journal of Planning Education and Research*, 36(3), 333–348.
- Balaji, M., Chakraborty, A. & Mandal, M. (2018) Changes in tropical cyclone activity in north Indian Ocean during satellite era (1981–2014). *International Journal of Climatology*, 38, 2819–2837.
- Bandyopadhyay, S. et al. (2018) *Cyclonic Storm Landfalls in Bangladesh, West Bengal and Odisha, 1877–2016: A Spatiotemporal Analysis*. The World Bank.
- Bates, P.D., Horritt, M.S. & Fewtrell, T.J. (2010) A simple inertial formulation of the shallow water equations for efficient two-dimensional flood inundation modelling. *Journal of Hydrology*, 387(1–2), 33–45.
- Bern, C. et al. (1993) Risk factors for mortality in the Bangladesh cyclone of 1991. *Bulletin of the World Health Organization*, 71(1), 73.
- Boke-Olen, N., Abdi, A.M., Hall, O. & Lehsten, V. (2017) High-resolution African population projections from radiative forcing and socio-economic models, 2000 to 2100. *Scientific Data*, 4, 160130.
- Carrère, L., Lyard, F., Cancet, M., Guillot, A. & Roblou, L. (2013) FES 2012: A new global tidal model taking advantage of nearly 20 years of altimetry. In: *20 years of progress in radar altimetry*. Vol. 710.
- Emanuel, K. & Rotunno, R. (2011) Self-stratification of tropical cyclone outflow. Part I: Implications for storm structure. *Journal of the Atmospheric Sciences*, 68(10), 2236–2249.
- Chen, J. & Mueller, V. (2018) Coastal climate change, soil salinity and human migration in Bangladesh. *Nature Climate Change*, 8(11), 981–985.
- Chowdhury, M. et al. (1992) *Cyclone aftermath: Research and directions for the future. From crisis to development: Coping with disasters in Bangladesh*. Dhaka Bangladesh: University Press Ltd, pp. 101–33.
- Church, J.A. et al. (2013): Sea level change. In: Stocker, T.F., Qin, D., Plattner, G.K., Tignor, M., Allen, S.K., Boschung, J., Nauels, A., Xia, Y., Bex, V. & Midgley, P.M. (Eds.) *Climate change 2013: The physical science basis. Contribution of working group I to the fifth assessment report of the intergovernmental panel on climate change*. Cambridge, United Kingdom and New York, NY, USA: Cambridge University Press.
- Dasgupta, S., Huq, M., Khan, Z.H., Ahmed, M.M.Z., Mukherjee, N., Khan, M.F. & Pandey, K. (2014) Cyclones in a changing climate: The case of Bangladesh. *Climate and Development*, 6(2), 96–110.
- Dasgupta, S., Laplante, B., Murray, S. & Wheeler, D. (2011) Exposure of developing countries to sea-level rise and storm surges. *Climatic Change* 106(4), 567–579.
- Dastagir, M.R. (2015) Modeling recent climate change induced extreme events in Bangladesh: A review. *Weather and Climate Extremes*, 7(2015), 49–60.
- de Almeida, G.A.M. & Bates, P. (2013) Applicability of the local inertial approximation of the shallow water equations to flood modeling. *Water Resources Research*, 49, 4833–4844.
- Devries, B., Huang, C., Armston, J., Huang, W., Jones, J.W. & Lang, M.W. (2020) Rapid and robust monitoring of flood events using Sentinel-1 and Landsat data on the Google Earth Engine. *Remote Sensing of Environment*, 240, 111664.
- Emanuel, K. (2017) Assessing the present and future probability of Hurricane Harvey's rainfall. *Proceedings of the National Academy of Sciences*, 114(48), 12681–12684.
- Eyring, V. et al. (2016) Overview of the Coupled Model Intercomparison Project Phase 6 (CMIP6) experimental design and organization. Geoscientific Model Development (Online)9.LLNL-JRNL-736881.
- Facebook Connectivity Lab and Center for International Earth Science Information Network - CIESIN - Columbia University. (2016) High Resolution Settlement Layer (HRSL). Source imagery for HRSL © 2016 DigitalGlobe. Available at: <https://data.humdata.org/> (Accessed 21/05/2020)
- Fredrick, T. et al. (2015) Cholera outbreak linked with lack of safe water supply following a tropical cyclone in Pondicherry, India, 2012. *Journal of Health, Population, and Nutrition*, 33(1), 31.

- Fritz, H.M., Blount, C.D., Thwin, S., Thu, M.K. & Chan, N. (2009) Cyclone Nargis storm surge in Myanmar. *Nature Geosci*, 2, 448–449. <https://doi.org/10.1038/ngeo558>
- GADM (2020) GADM database of Global Administrative Areas, version 4.0.
- Gao, J. (2017) Downscaling global spatial population projections from 1/8-degree to 1-km grid cells. National Center for Atmospheric Research. <https://doi.org/10.5065/D60Z721H>
- Greatbatch, R.J. (1994) A note on the representation of steric sea level in models that conserve volume rather than mass, *J. Geophys. Res.*, 99(C6), 12767–12771, <https://doi.org/10.1029/94JC00847>.
- Hawker, L., Neal, J., & Bates, P. (2019) Accuracy assessment of the TanDEM-X 90 Digital Elevation Model for selected floodplain sites. *Remote Sensing of Environment*, 232, 111319.
- Hoegh-Guldberg, O., Jacob, D., Bindi, M., Brown, S., Camilloni, I. et al. (2018) Impacts of 1.5 C global warming on natural and human systems. *Global warming of 1.5 C. An IPCC special report*.
- Holland, G.J. (1980) An analytic model of the wind and pressure profiles in hurricanes. *Monthly Weather Review*, 108(8), 1212–1218.
- Hossain, M.N. (2015) Analysis of human vulnerability to cyclones and storm surges based on influencing physical and socioeconomic factors: Evidences from coastal Bangladesh. *International Journal of Disaster Risk Reduction*, 13(2015), 66–75.
- Hurtt, G.C., Chini, L., Sahajpal, R., Froking, S., Bodirsky, B.L., Calvin, K. et al. (2020) Harmonization of global land use change and management for the period 850–2100 (LUH2) for CMIP6. *Geoscientific Model Development*, 13(11), 5425–5464.
- Huq, S., Roberts, E. & Fenton, A. (2013) Loss and damage. *Nature Climate Change*, 3(11), 947–949.
- IIASA, I.I.F.A.S.A. (2018) *SSP Public Database Version 2.0*. SSP Public Database.
- Islam, T. & Peterson, R. (2009) Climatology of landfalling tropical cyclones in Bangladesh 1877–2003. *Natural Hazards*, 48(1), 115–135.
- James, R., Otto, F., Parker, H., Boyd, E., Cornforth, R., Mitchell, D. & Allen, M. (2014) Characterizing loss and damage from climate change. *Nature Climate Change*, 4(11), 938.
- Jiang, L. & O'Neill, B.C. (2017) Global urbanization projections for the Shared Socioeconomic Pathways. *Global Environmental Change*, 42, 193–199.
- Jones, B. & O'Neill, B.C. (2016) Spatially explicit global population scenarios consistent with the shared socioeconomic pathways. *Environ. Res. Lett.*, 11, 084003. <https://doi.org/10.1088/1748-9326/11/8/084003>.
- Khan, M.J.U. (2020) Digitized flood location dataset during cyclone Amphan from newspaper survey. Zenodo. <http://doi.org/10.5281/zenodo.4086103>
- Khan, M.J.U., Durand, F., Bertin, X., Testut, L., Krien, Y., Islam, A.K.M.S. et al. (2021). Towards an efficient storm surge and inundation forecasting system over the Bengal delta: chasing the Super-cyclone Amphan. *Nat. Hazards Earth Syst. Sci.*, 21, 2523–2541.
- Knutson, T.R., McBride, J.L., Chan, J., Emanuel, K., Holland, G., Landsea, C. et al. (2010) Tropical cyclones and climate change. *Nature geoscience* 3(3), 157–163.
- Knutson, T., Camargo, S.J., Chan, J.C.L., Emanuel, K., Ho, C.-H., Kossin, J. et al. (2020) Tropical cyclones and climate change assessment. Part 2: Projected response to anthropogenic warming. *Bulletin of the American Meteorological Society*, 101(3), 302–322. <https://doi.org/10.1175/BAMS-D-18-0194.1>.
- Krishna, K.M. (2009) Intensifying tropical cyclones over the North Indian Ocean during summer monsoon—Global warming. *Global and Planetary Change*, 65(1–2), 12–16.
- Kulp, S.A. & Strauss, B. (2019) New elevation data triple estimates of global vulnerability to sea-level rise and coastal flooding. *Nature Communications*, 10(1), 1–12.
- Lewis, M., Bates, P., Horsburgh, K., Neal, J. & Schumann, G. (2013) A storm surge inundation model of the northern Bay of Bengal using publicly available data. *Quarterly Journal of the Royal Meteorological Society*, 139, 358–369.
- Li, Z., Yu, W., Li, T., Murty, V.S.N. & Tangang, F. (2013) Bimodal character of cyclone climatology in the Bay of Bengal modulated by monsoon seasonal cycle. *Journal of Climate*, 26(3), 1033–1046.
- Lin, N., Emanuel, K., Oppenheimer, M. & Vanmarcke, E. (2012) Physically based assessment of hurricane surge threat under climate change. *Nature Climate Change*, 2(6), 462–467.
- Lin, N., Emanuel, K. (2016) Grey swan tropical cyclones. *Nature Climate Change*, 6, 106–111. <https://doi.org/10.1038/nclimate2777>
- Lin, N., Kopp, R.E., Horton, B.P. & Donnelly, J.P. (2016) Hurricane Sandy's flood frequency increasing from year 1800 to 2100. *Proceedings of the National Academy of Sciences*, 113(43), 12071–12075.
- Matthews, T., Wilby, R. & Murphy, C. (2019) An emerging tropical cyclone–deadly heat compound hazard. *Nature Climate Change*, 9(8), 602–606.
- Merkens, J.-L. et al. (2016) Gridded population projections for the coastal zone under the shared socioeconomic pathways. *Glob. Planet. Chang.*, 145, 57–66. <https://doi.org/10.1016/j.gloplacha.2016.08.009232>
- Michra, A.K. & Vanganuru, N. (2020) Monitoring a tropical super cyclone Amphan over Bay of Bengal and nearby region in May 2020. *Remote Sensing Applications: Society and Environment*, 20, 100408.
- Milne, G.A., Gehrels, W.R., Hughes, C.W. & Tamisiea, M.E. (2009): Identifying the causes of sea-level change. *Nat. Geosci.*, 2, 471–478, <https://doi.org/10.1038/ngeo544>.
- Mitchell, D., James, R., Forster, P.M., Betts, R.A., Shiogama, H. & Allen, M. (2016) Realizing the impacts of a 1.5 C warmer world. *Nature Climate Change*, 6(8), 735.
- Mohapatra, M., Srivastava, A.K., Balachandran, S. & Geetha, B., (2017) Inter-annual variation and trends in tropical cyclones and monsoon depressions over the north Indian Ocean. In: M. N. Rajeevan & S. Nayak (Eds.), *Observed climate variability and change over the Indian region*. Springer, pp. 89–106.
- NAS; National Academies of Sciences, Engineering, and Medicine. (2016) *Attribution of extreme weather events in the context of climate change*. Washington, DC: The National Academies Press. <https://doi.org/10.17226/21852>.
- Nicholls, R.J. et al. (2008) Ranking port cities with high exposure and vulnerability to climate extremes: exposure estimates. OECD Publishing.
- Oppenheimer, M. et al. (2019) Sea level rise and implications for low lying Islands, coasts and communities. In: H.-O. Pörtner et al. (Eds.), *IPCC special report on the ocean and cryosphere in a changing climate*. In press.
- Patricola, C.M. & Wehner, M. (2018) Anthropogenic influences on major tropical cyclone events. *Nature*, 563(7731), 339–346.
- Peltier, W.R., Argus, D.F. & Drummond, R. (2015) Space geodesy constrains ice-age terminal deglaciation: The global ICE-6G_C

- (VM5a) model. *J. Geophys. Res. Solid Earth*, 120, 450–487, <https://doi.org/10.1002/2014JB011176>.
- Phillips, C.A. et al. (2020) Compound climate risks in the COVID-19 pandemic. *Nature Climate Change*, 1–3.
- Rahman, S. et al. (2019) Impact of sea level rise on cyclonic storm surges in Ganges-Brahmaputra-Meghna Delta. *Journal of Earth System Science*, 128(6), 145.
- Riahi, K., van Vuuren, D.P., Kriegler, E., Edmonds, J., O'Neill, B.C., Fujimori, S., et al (2017) The Shared Socioeconomic Pathways and their energy, land use, and greenhouse gas emissions implications: An overview. *Global Environmental Change*, 42, 153–168.
- Risser, M.D. & Wehner, M.F. (2017) Attributable human-induced changes in the likelihood and magnitude of the observed extreme precipitation during Hurricane Harvey. *Geophysical Research Letters*, 44(24), 12–457.
- Samir, K. & Lutz, W. (2017) The human core of the shared socioeconomic pathways: Population scenarios by age, sex and level of education for all countries to 2100. *Glob Environ Change*, 42, 181–192.
- Sampson, C.C., Smith, A.M., Bates, P.D., Neal, J.C., Alfieri, L. & Freer, J.E. (2015) A high resolution global flood hazard model. *Water Resources Research*, 51(9), 7358–7381.
- Sehgal, S.C., Sugunan, A.P. & Vijayachari, P. (2002) Outbreak of leptospirosis after the cyclone in Orissa. *National Medical Journal of India*, 15(1), 22–23.
- Shultz, J.M., Russell, J. & Espinel, Z. (2005) Epidemiology of tropical cyclones: The dynamics of disaster, disease, and development. *Epidemiologic reviews* 27(1), 21–35.
- Shultz, J.M., Kossin, J.P., Ali, A., Borowy, V., Fugate, C., Espinel, Z. et al. (2020) Superimposed threats to population health from tropical cyclones in the prevaccine era of COVID-19. *The Lancet Planetary Health*, 4(11), e506–e508.
- Singha, M., Dong, J., Sarmah, S., You, N., Zhou, Y., Zhang, G. et al. (2020) Identifying floods and flood-affected paddy rice fields in Bangladesh based on Sentinel-1 imagery and Google Earth Engine. *ISPRS Journal of Photogrammetry and Remote Sensing*, 166, 278–293.
- Smith, A., Bates, P.D., Wing, O., Sampson, C., Quinn, N. & Neal, J. (2019) New estimates of flood exposure in developing countries using high-resolution population data. *Nature Communications*, 10(1), 1–7.
- Sovacool, B.K. (2018) Bamboo beating bandits: Conflict, inequality, and vulnerability in the political ecology of climate change adaptation in Bangladesh. *World Development*, 102, 183–194.
- Sultana, P. & Thompson, P. (2017) Adaptation or conflict? Responses to climate change in water management in Bangladesh. *Environmental Science & Policy*, 78, 149–156.
- Van Oldenborgh, G.J., Van Der Wiel, K., Sebastian, A., Singh, R., Arrighi, J., Otto, F. et al. (2017) Attribution of extreme rainfall from Hurricane Harvey, August 2017. *Environmental Research Letters*, 12(12), 124009.
- Vosper, E., Mitchell, D. & Emanuel, K. (2020) Extreme hurricane rainfall affecting the Caribbean mitigated by Paris Agreement goals. *Environmental Research Letters*, 15, 104053.
- Walsh, K.J.E., Camargo, S.J., Knutson, T.R., Kossin, J., Lee, T.-C., Murakami, H. et al. (2019) Tropical cyclones and climate change. *Tropical Cyclone Research and Review*, 8(4), 240–250.
- Webster, P.J. (2013) Improve weather forecasts for the developing world. *Nature*, 493(7430), 17–19.
- Wehner, M. & Sampson, C. (2021) Attributable human-induced changes in the magnitude of flooding in the Houston, Texas region during Hurricane Harvey. *Climatic Change*, 166(1), 1–13.
- Wing, O.E.J., Sampson, C.C., Bates, P.D., Quinn, N., Smith, A.M. & Neal, J.C. (2019) A flood inundation forecast of Hurricane Harvey using a continental-scale 2D hydrodynamic model. *Journal of Hydrology X*, 4, 100039.
- Woodruff, J.D., Irish, J.L. & Camargo, S.J. (2013) Coastal flooding by tropical cyclones and sea-level rise. *Nature*, 504(7478), 44–52.
- Yamazaki, D., Ikeshima, D., Tawatari, R., Yamaguchi, T., O'Loughlin, F., Neal, J.C. et al. (2017) A high-accuracy map of global terrain elevations. *Geophysical Research Letters*, 44, 5844–5853.
- Yamazaki, D., Trigg, M.A. & Ikeshima, D. (2015) Development of a global ~90 m water body map using multi-temporal Landsat images. *Remote Sensing of Environment*, 171, 337–351.
- Yanase, W., Satoh, M., Taniguchi, H. & Fujinami, H. (2012) Seasonal and intraseasonal modulation of tropical cyclogenesis environment over the Bay of Bengal during the extended summer monsoon. *Journal of Climate*, 25(8), 2914–2930.
- Yu, J. & Wang, Y. (2009) Response of tropical cyclone potential intensity over the north Indian Ocean to global warming. *Geophysical Research Letters*, 36(3).
- Zhang, Y., Ye, F., Stanev, E.V. & Grashorn, S. (2016) Seamless cross-scale modeling with SCHISM. *Ocean Modelling*, 102, 64–81. <https://doi.org/10.1016/j.ocemod.2016.05.002>

SUPPORTING INFORMATION

Additional supporting information can be found online in the Supporting Information section at the end of this article.

How to cite this article: Mitchell, D., Hawker, L., Savage, J., Bingham, R., Lord, N.S., Khan, M.J.U. et al. (2022) Increased population exposure to Amphan-scale cyclones under future climates. *Climate Resilience and Sustainability*, 1, e36. <https://doi.org/10.1002/cli2.36>